PROFESSOR HOLGER PUCHTA (Orcid ID: 0000-0003-1073-8546)

Article type : Technical Advance

Live cell CRISPR-imaging in plants reveals dynamic telomere movements

Steven Dreissig¹, Simon Schiml², Patrick Schindele², Oda Weiss¹, Twan Rutten¹, Veit Schubert¹, Evgeny Gladilin¹, Michael Florian Mette^{1,3}, Holger Puchta^{*,2} & Andreas Houben^{*,1}

¹Leibniz Institute of Plant Genetics and Crop Plant Research (IPK), Gatersleben, 06466 Stadt Seeland, Germany

²Botanical Institute, Karlsruhe Institute of Technology, POB 6980, 76049 Karlsruhe, Germany

³Current address: King Abdullah University of Science & Technology, Thuwal 23955-6900, Kingdom of Saudi Arabia

*corresponding authors:

contact: houben@ipk-gatersleben.de

tel.: +49394825486

fax: +49394825137

This article has been accepted for publication and undergone full peer review but has not been through the copyediting, typesetting, pagination and proofreading process, which may lead to differences between this version and the Version of Record. Please cite this article as doi: 10.1111/tpj.13601

This article is protected by copyright. All rights reserved.

contact: holger.puchta@kit.edu

tel.: +4972160843833

fax: +4972160844874

email addresses of all other authors:

dreissig@ipk-gatersleben.de, simon.schiml@kit.edu, patrick.schindele@kit.edu,

weisso@ipk-gatersleben.de, rutten@ipk-gatersleben.de, schuberv@ipk-gatersleben.de,

gladilin@ipk-gatersleben.de, florian.mette@kaust.edu.sa

Running title: CRISPR-imaging of plant telomeres

Key words: CRISPR-dCas9, live cell imaging, telomeres, chromatin dynamics, nucleus,

Nicotiana benthamiana

Summary

Elucidating the spatio-temporal organization of the genome inside the nucleus is

imperative to understand the regulation of genes and non-coding sequences during

development and environmental changes. Emerging techniques of chromatin imaging

promise to bridge the long-standing gap between sequencing studies which reveal

genomic information and imaging studies that provide spatial and temporal information

of defined genomic regions. Here, we demonstrate such an imaging technique based on

two orthologues of the bacterial CRISPR-Cas9 system. By fusing eGFP/mRuby2 to the

catalytically inactive version of Streptococcus pyogenes and Staphylococcus aureus

Cas9, we show robust visualization of telomere repeats in live leaf cells of Nicotiana

This article is protected by copyright. All rights reserved.

benthamiana. By tracking the dynamics of telomeres visualized by CRISPR-dCas9, we reveal dynamic telomere movements of up to 2 µm within 30 minutes during interphase. Furthermore, we show that CRISPR-dCas9 can be combined with fluorescence-labelled proteins to visualize DNA-protein interactions *in vivo*. By simultaneously using two dCas9 orthologues, we pave the way for imaging of multiple genomic loci in live plants cells. CRISPR-imaging bears the potential to significantly improve our understanding of the dynamics of chromosomes in live plant cells.

Introduction

The spatial and temporal organization of genomes is important for maintaining and regulating cell functions such as gene expression, DNA replication and repair, and proper segregation of genetic material during cell division. Elucidating how the genome is spatio-temporally organised inside the nucleus is imperative to understand how genes and non-coding sequences are regulated during development. Mapping the functional organization of the genome can be achieved by visualizing interactions between different genomic elements in living cells. While fluorescence-tagged nuclear proteins can be readily imaged in living plant cells, *in vivo* visualization of defined DNA sequences is technically difficult. Fluorescent *in situ* hybridization (FISH), a well-established tool to map DNA sequences, relies on fixed tissue samples and cannot be used to visualize dynamic processes. Further, FISH requires cell fixation and a DNA denaturation step which may result in an altered chromatin structure (Boettiger *et al.* 2016, Kozubek *et al.* 2000).

Live cell labelling of specific genomic loci has been achieved by the application of a directly repeated *lac* operator sequence and its detection with a GFP-lac repressor protein (Kato and Lam 2001). However, this system is based on the random insertion of an artificial sequence into the genome. Live imaging of endogenous genomic regions became possible with the application of fluorescence-tagged zinc-finger proteins. A zinc-finger-GFP protein was designed to recognize a 9 bp sequence within the centromeric 180 bp tandem repeat of Arabidopsis thaliana (Lindhout et al. 2007). Despite the numerous uses of engineered zinc finger proteins for genome editing, the potential of this technology has not yet been fully exploited for chromatin imaging. The discovery of the Xanthomonas-based DNA-binding domain (Boch et al. 2009) which can be engineered to bind specific DNA sequences initiated the development of transcription activator-like effectors (TALEs) fused with fluorescence proteins (Ma et al. 2013). While fluorescent TALEs were successfully used to trace genomic loci in nonplant organisms [reviewed in Chen et al. (2016a)], their application in plants has only recently been shown (Fujimoto et al. 2016).

The discovery of the type II clustered regularly interspaced short palindromic repeats (CRISPR)--associated caspase 9 (Cas9) system derived from *Streptococcus pyogenes* revolutionized the field of targeted genome editing in eukaryotes (Jinek *et al.* 2012). Cas9 nuclease based genome engineering has become a routine technology for many plant species [reviewed in Pacher and Puchta (2016)]. However, the full potential of this technology reaches far beyond the controlled induction of mutations. The Cas9 nuclease can be transformed into a site-specific DNA binding protein by two point mutations, which can be fused with different protein domains. Thus, it should in principle

be possible to target any kind of enzymatic activity to any genomic site of interest (Puchta 2016a). Recently, nuclease-deficient derivatives (dCas9) were used to modify gene expression in many model organisms including plants (Piatek *et al.* 2015, Qi *et al.* 2013). Further, by fusing dCas9 with GFP, the CRISPR/dCas9 system has been used to label genomic loci in live mammalian cells (Anton *et al.* 2014, Chen *et al.* 2013). Multicolour CRISPR-dCas9 imaging became possible by the application of dCas9 orthologues from different bacteria species, like *Neisseria meningitidis* (NmCas9), *Streptococcus thermophilus* (St1Cas9), and *Staphylococcus aureus* (Chen *et al.* 2016b, Ma *et al.* 2015). The discovery of the Cas9-like activities of the Cpf1 protein derived from *Acidaminococcus* and *Lachnospiraceae* (Zetsche *et al.* 2015) may further expand the palette of multicolour CRISPR-dCas9 imaging. More importantly, orthologues of SpCas9, such as St1-Cas9 and Sa-Cas9 have been confirmed to be functional in plants (Steinert *et al.* 2015).

In the current study, we describe the development of CRISPR-dCas9 for live cell imaging in plants based on two Cas9 orthologues derived from *Streptococcous* pyogenes (Sp-dCas9) and *Staphylococcus aureus* (Sa-dCas9). We demonstrate reliable imaging of telomere repeats in living cells of *Nicotiana benthamiana* and pave the way for potential visualization of multiple genomic loci. Furthermore, we show that CRISPR-dCas9 can be combined with fluorescence-labelled proteins to investigate DNA-protein interactions *in vivo*.

Results & Discussion

CRISPR-dCas9 enables visualization of tandem repeats in live plant cells

To establish live cell imaging by CRISPR-dCas9 in plants, we introduced a point mutation in the RuvC1 and HNH nuclease domains (D10A and H841A) in two Cas9 orthologues derived from *Streptococcus pyogenes* (Sp-dCas9) and *Staphylococcus aureus* (Sa-dCas9) which were previously used for targeted mutagenesis in *A. thaliana* (Fauser *et al.* 2014, Steinert, Schiml, Fauser and Puchta 2015), rendering the Cas9 protein catalytically inactive. Multiple copies of fluorescence proteins, either eGFP or mRuby2, were fused to the C-terminal end of each dCas9 variant (Figure 1a).

To test the functionality of CRISPR-dCas9 for live cell imaging in plants, we imaged the telomeres of *Nicotiana benthamiana* in leaf cells. *Nicotiana* telomeres are composed of 60 - 160 kb-long arrays of TTTAGGG repeats (Fajkus *et al.* 1995). These tandemly repeated DNA sequences allow the binding of many dCas9 proteins at the same locus by a single sgRNA sequence. To target telomeric repeats, we constructed a 20 nucleotide sgRNA complementary to the TTTAGGG telomere sequence starting with a 'G' at the 5'-end (sgRNA-telomere, Figure 1b). The 5'-G nucleotide was selected as the employed *A. thaliana* U6-26 promoter requires it to initiate transcription (Belhaj *et al.* 2013).

We used infiltration by *A. tumefaciens* to transiently express Sp-dCas9 and sgRNA-telomere in leaf cells. As a negative control, the same dCas9 construct was infiltrated without a specific sgRNA. After 2-4 days, bright fluorescence puncta were observed in addition to a weak unspecific background labelling of the nucleus and in particular of the nucleolus (Figure 2a). A similar unspecific labelling of the nucleolus caused by CRISPR-

dCas9 was observed in previous studies (Chen, Gilbert, Cimini, Schnitzbauer, Zhang, Li, Park, Blackburn, Weissman, Qi and Huang 2013, Zhou et al. 2017). In negative controls, only a weak unspecific labelling of the nucleus was observed (Figure 2b). In live interphase nuclei, we detected an average of 21.75 telomere signals by CRISPRimaging (n=50 nuclei). To confirm telomere-specificity of the fluorescence signals and to quantify the efficiency of dCas9 to label telomeres, we analysed the co-localization of dCas9 and telomeres by immuno-fluorescence and FISH (Figure 2c-2e). On average, 27 signals were detected by immuno-fluorescence labelling of dCas9 which amounts to 78% of all telomeres detected by FISH (Figure 2e). We observed an average of 35 telomere FISH signals which indicates a certain degree of telomere clustering since the expected number of telomeres based on a chromosome complement of 2n = 38 would be 76 in 2C nuclei (Supplementary File 1). Notably, a similar localization pattern was observed in wild-type leaf interphase nuclei (Supplementary File 2) although we detected a higher number of telomere signals (average=53, n=30). We then used dCas9 without introducing a specific sgRNA as a control and detected an average of 42 signals (n=30). Since the detectable number of telomeres appears to be highly variable in N. benthamiana leaf nuclei, we conclude that mainly nuclei with clustered telomeres were visualized in our experimental system. A higher number of CRISPR-dCas9 signals were observed in fixed cells after immuno-fluorescence labelling compared to live cells which might be a result of the improved detection efficiency of the GFP antibody. The intensity of individual hybridization signals varied most likely due to chromosomespecific differences in telomere repeat number and fusion of chromosome ends. Importantly, we observed a positive correlation ($\rho = 0.84$, $r^2 = 0.7$, n = 30) between FISH

and CRISPR-imaging regarding the intensity and size of hybridization signals (Figure 2g).

Imaging of telomeres by CRISPR-dCas9 reveals long range telomere dynamics

We then attempted to explore the possibility to visualize telomere movements in a live nucleus by CRISPR-imaging. To visualize the nuclear envelope in addition to telomeres, we used the nuclear egress protein of the human cytomegalovirus pUL50 fused to GFP which was previously shown to localize to the *N. benthamiana* nuclear envelope (Lamm *et al.* 2016). Individual nuclei were observed *in vivo* for a total of 30 minutes and z-stacks were acquired in 1 minute intervals. We observed stable fluorescence over the entire period of time.

To investigate whether there is stable association of dCas9 to its target sequence or rapid turnover, we conducted FRAP (fluorescence recovery after photobleaching) experiments. After bleaching individual dCas9 clusters of three nuclei, we found no significant fluorescence recovery over a period of 30 minutes (Figure 3). This indicates a stable association of dCas9 to its target sequence which is in agreement with previous reports showing an average target residence time of more than 3 hours in mammalian cells (Ma *et al.* 2016, Qin *et al.* 2017).

Several dynamic subcellular movements were observed. First, entire nuclei showed movements in all three dimensions over time. Within those nuclei, however, telomeres tended to follow these movements but also changed their position relative to each other (Supplementary File 3) and were localized in proximity to the nuclear envelope which was shown by a mean normalized radial distance of telomeres of 0.74 (Figure 4a,

Supplementary File 4). To quantify these dynamics, we tracked the spatial movements of telomeres over the entire period of time and measured their mean square displacement (MSD) (Figure 4b, Supplementary File 5, Supplementary File 6). By tracking single telomere clusters, we observed confined diffusion of telomere clusters as well as long range movements which results in a high standard deviation of the MSD. To reveal these variations in a representative nucleus, we calculated absolute changes in inter-telomere distance over time (Figure 4c, d). Within 30 minutes, individual telomeres changed their distance to each other by up to $\pm 2 \mu m$ (average diameter of the nucleus = 15.12 µm, n=12). Compared to an average inter-telomeres distance of 8.1 µm, these changes can amount to a maximum of 24.7%. Similar observations were made previously in A. thaliana by labelling telomeres via fluorescent TALEs (Fujimoto, Sugano, Kuwata, Osakabe and Matsunaga 2016). Compared to Fujimoto, Sugano, Kuwata, Osakabe and Matsunaga (2016), however, we did not observe an active formation of telomere clusters. This might be related to differences in interphase telomere dynamics between A. thaliana root cells and N. benthamiana leaf cells rather than CRISPR-dCas9 having a negative effect on telomere dynamics since both MSD curves are similar. Telomere dynamics during interphase might be related to transcription of telomeric tandem repeats (Koo et al. 2016), telomerase activity (Schrumpfova et al. 2016), or positional silencing by telomeres (Cryderman et al. 1999, Gottschling et al. 1990, Nimmo et al. 1994). Similar long range chromatin dynamics of specific interstitial chromosomal regions were previously described based on fixed A. thaliana cells (Schubert et al. 2014). Our results reveal that long range chromatin movements can occur over a short period of time which we suggest is highly relevant

for chromatin conformation capture studies [reviewed in Bonev and Cavalli (2016)] aiming to look at such interactions. We conclude that CRISPR-dCas9 is a robust system to reveal the dynamics of telomeres in live plant cells.

Visualization of DNA-protein dynamics at plant telomeres

Since CRISPR-dCas9 is a tool to visualize specific DNA sequences, it can be combined with other methods, e.g. fluorescence-labelled proteins, to study the dynamics of DNA-protein interactions. As an example, we attempted to visualize telomeric DNA by CRISPR-dCas9 and the telomeric repeat binding protein 1 (TRB1) in live leaf cells of *Nicotiana benthamiana*. TRB1 was previously described to be located at plant telomeres and interact with TERT (telomerase reverse transcriptase), although not all telomeres are bound by TRB1 (Dvorackova *et al.* 2010, Schrumpfova *et al.* 2014). Interestingly, telomeres in yeast, ciliates, mammals and plants may form 3' overhangs. However, in plants, blunt-ended telomeres and telomeres with 3' overhangs may appear in the same cell and only telomeres exhibiting 3' overhangs are bound by TRB1.

We simultaneously expressed Sp-dCas9-mRuby, sgRNA-telomere and TRB1-GFP in leaf cells to visualize the dynamic relationship between the telomeric repeats of all chromosomes and the proportion of which is bound by TRB1. On average, we detected 30 CRISPR-dCas9 signals resembling telomeres out of which 26.3 (87.6%) were simultaneously bound by TRB1 (Figure 5). This indicates that most telomeres in *N. benthamiana* form 3' overhangs and only a small proportion of blunt-ended telomeres is present during interphase. Our results demonstrate that CRISPR-dCas9 can be used to

visualize specific DNA sequences in combination with fluorescently tagged proteins interacting with those DNA sequences. We hypothesize that this principle can be expanded to investigate spatio-temporal gene expression patterns, e.g. by visualizing DNA sequences and transcription factors, as well as other DNA-protein interactions such as the loading of specific histone variants to certain genomic regions (e.g. CENH3 and centromeric DNA).

Comparing the efficiency of two dCas9 orthologues for imaging of telomeres

In addition to Sp-dCas9 derived from S. pyogenes, we used Sa-dCas9 derived from S. aureus to visualize telomeres, compare their efficiency, and potentially pave the way for simultaneous imaging of multiple genomic loci in plants. The protospacer-adjacent motif (PAM) required by Sa-dCas9 (NGGGT) allowed us to use the same sgRNA as for SpdCas9. In contrast to Sp-dCas9, the sgRNA scaffold sequence of Sa-dCas9 as well as the size of the complex itself differs (Sa-dCas9 = 1064 amino acids vs Sp-dCas9 = 1380 amino acids) which could have an effect on its efficiency (Chen et al. 2016c). In previous experiments, we showed that in plant cells Sp-Cas9 and Sa-Cas9 are only forming a complex with their respective sgRNA and not with the sgRNA of the other orthologue (Steinert, Schiml, Fauser and Puchta 2015). Compared to Sp-dCas9 detecting 78% of all telomeres, using Sa-dCas9 we were able to detect 85.5 % of all telomeres when both variants were analysed separately. We then used both variants Sp-dCas9-mRuby2 and Sa-dCas9-eGFP simultaneously to visualize telomeres and demonstrate the potential application of different dCas9 orthologues for multiple genomic loci. When combined, both variants showed almost complete co-localization

indicating no significant difference in their efficiency to detect telomeres (Figure 6). We conclude that both Sp-dCas9 and Sa-dCas9 can be used simultaneously to visualize tandem repeats in live plant cells. Thus, by using different Cas9 or Cpf1 orthologues fused to different florescence proteins multidimensional live imaging in single cells might become a reality in the long run (Puchta 2016b). For tandem repetitive sequences, a single sgRNA may be sufficient for CRISPR-imaging whereas labelling of non-repetitive loci (spanning a 5 kb region) may require simultaneous expression of at least 30 sgRNAs (Chen, Gilbert, Cimini, Schnitzbauer, Zhang, Li, Park, Blackburn, Weissman, Qi and Huang 2013). More recently, an entire human chromosome was visualized by CRISPR-imaging by using at least 485 non-repetitive sgRNAs at the same time (Zhou, Wang, Tian, Gao, Huang, Wei and Xie 2017). An alternative approach is to tether fluorescent RNA-binding proteins to the sgRNA through aptamer fusions thereby transforming the sgRNA into a scaffold RNA which contains information about the target locus and the type of fluorescence (Shao et al. 2016). These recent developments may further improve CRISPR-imaging in plants and potentially enable us to visualize single genomic loci.

Experimental procedures

T-DNA construction

All constructs are based on our previously described vector pCAS9-TPC (Fauser *et al.*, 2014). For the two Cas9 orthologues from *S. pyogenes* (Sp) and *S. aureus* (Sa), respective dCas9 versions were generated by two consecutive rounds of site-directed mutagenesis, thereby introducing the two point mutations (D10A / H840A for Sp-dCas9

and D10A / N580A for Sa-dCas9). Plasmids encoding for eGFP (pSiM24-eGFP) and mRuby2 (pcDNA3-mRuby2) were obtained from Addgene (www.addgene.com). dCas9 and fluorescence protein (FP) sequences were generated with primers containing homologous flanks for subsequent Gibson Assembly cloning into the pCAS9-TP backbone (for a full list of primers, see Supplementary File 7). The stop codons of the dCas9 and the first two FP sequences were removed to generate a continuous ORF, harbouring the respective dCas9 orthologue followed by a 3-fold fusion of the appropriate FP sequence. The dCas9 sequence and the FP fusion as well as the single FP sequences were linked via a GS-rich linker, respectively. Protospacers were allowed to self-anneal and the resulting 4-bp overhangs were used for subsequent ligation into the respective pChimera vector via *BbsI* restriction sites. The customised RNA chimeras were then ligated into the respective dCas9 vectors via *MluI* restriction sites. The Cas9 constructs developed in this study are available on request to HP.

Protospacer design

Protospacer sequences were selected based on the respective protospacer adjacent motif (PAM) sequence of each dCas9 orthologue, namely SpdCas9 and SadCas9, and synthesized as oligonucleotides with appropriate 4-bp 5′-overhangs for cloning into the respective pChimera vector. The telomere-specific protospacer (5′-GGGTTTAGGGTTTAGGGTTT-3′) is based on the *Arabidopsis*-type telomere repeat sequence 5′-(TTTAGGG)(n)-3′. Due to the presence of both Sp-dCas9 (5′-NGG-3′) and Sa-dCas9 (5′-NNGGGT-3′) PAM sequences in the telomere repeat sequence, both

variants were used to label telomeres which allowed us to compare these two orthologues.

Transient transformation of N. benthamiana

All CRISPR-dCas9 constructs, TRB1-GFP (Schrumpfova, Vychodilova, Dvorackova, Majerska, Dokladal, Schorova and Fajkus 2014), and pUL50-GFP (Lamm, Link, Wagner, Milbradt, Marschall and Sonnewald 2016) were separately transformed into *Agrobacterium tumefaciens* strain GV3101 by electroporation. *Agrobacteria* containing Sp-dCas9, Sa-dCas9 and pUL50-GFP were cultured in YEB medium containing spectinomycin (100 μg/ml) and rifampicin (50 μg/ml). For TRB1-GFP, *Agrobacteria* were cultured in YEB medium containing kanamycin (100 μg/ml) and rifampicin (50 μg/ml). Transient transformation of *N. benthamiana* leaf cells was performed as described in Phan and Conrad (2016). For the transformation of multiple constructs, bacterial cultures with an OD between 1 - 1.3 were mixed in a 1:1 ratio prior to transformation. Plants were analysed 2-4 days after infiltration.

Immunofluorescence analysis and fluorescence in situ hybridization

2-3 days after leaf infiltration, nuclei were extracted by chopping a 1 cm² piece of leaf tissue in 1 ml chromosome isolation buffer (Dolezel *et al.* 2007) using a razor blade followed by filtration through a 35 μm nylon mesh and subsequent centrifugation onto a microscopic slide at 400 rpm for 5 minutes (Shandon, CytoSpin3). To confirm the specificity of each dCas9 construct, we conducted immunofluroresence staining against eGFP and mRuby2 in combination with fluorescence *in situ* hybridization (immuno-

FISH) against telomeres. Immuno-FISH was performed as described in Ishii *et al.* (2015). eGFP was detected with a polyclonal GFP antibody (Rockland, GFP antibody Dylight 488) in a 1:2,500 dilution. mRuby2 was detected with a primary RFP antibody (Chromotek, RFP antibody [5F8], 1:1000 dilution) generated in rats followed by an antirat secondary antibody (abcam, ab96889). To detect telomeres via FISH, we used 5'-Cy5 labelled oligonucleotides composed of the same DNA sequence as the respective protospacer (sgRNA-telomere, GGGTTTAGGGTTTAGGGTTT). A final probe concentration of 0.33 μM was used. Correct telomeric localization of our FISH probe was validated by application on *N. benthamiana* chromosomes (Supplementary file 1) prepared from flower buds using a protocol described by Sanchez Moran *et al.* (2001)

Microscopic analyses

To analyse co-localization between CRISPR-dCas9 imaging and FISH signals, images were acquired with an epifluorescence microscope BX61 (Olympus) using a cooled charge coupled device (CCD) camera (Orca ER, Hamamatsu) and analysed with ImageJ. A total of 50 nuclei was analysed by immuno-FISH to determine the efficiency of dCas9 to detect telomeres. The number of *in vivo* dCas9 signals was counted in 50 live nuclei to determine the *in vivo* labelling effiency. To analyse the co-localization of telomeres visualized by Sp-dCas9 and TRB1, a total of 43 nuclei was analysed by epifluorescence microscopy. Structured illumination microscopy (SIM) was applied on a representative sample using a 63x/1.4 Oil Plan-Apochromat objective of an Elyra PS.1 microscope system and the ZEN software (Carl Zeiss, Germany). Image stacks were captured separately for each fluorochrome using appropriate excitation and emission

filters. Maximum intensity projections were generated from the stacks of optical SIM sections through the specimens by the ZEN software (3D-rendering based on SIM image stacks was carried out using the Imaris 8.0 software (Bitplane).

For live cell imaging of telomeres, fluorescence signals were analysed 2-4 days after infiltration with *Agrobacterium tumefaciens* (see Transient transformation of *N. benthamiana*) by a LSM780 (Carl Zeiss, Germany). Infiltrated leaf areas were cut and mounted onto a microscopic slide. The distribution of fluorescence signals within the nucleus was recorded as Z-stacks (n=50 nuclei). For a co-distribution analysis, probes were excited with dual 488 nm and 561 nm laser lines in combination with a 488/561 nm beam splitter. eGFP emission was detected over a 490 – 540 nm range, mRuby2 emission was detected over a 570-620 nm range. Photospectrometric analysis of the fluorescence signal by means of the META-detector confirmed the identity of GFP and mRuby. Turn-over of Sp-dCas9-eGFP telomeric signals was investigated by FRAP analysis. After two pre-scans a region of interest of variable size was bleached. To achieve appropriate bleaching, the 488 nm laser line was set at 100% power with 25 iterations at scan speed 7. Fluorescence intensity was followed over 30 min in 1 min intervals.

Tracking of telomere signals and 3D image analysis

Telomere tracking based on time-lapse Z-stacks was conducted with the Imaris 8.0 software (Bitplane). Brightness was manually adjusted to detect all telomere clusters. Tracking was performed using the autoregression motion algorithm with a maximum distance of 20 µm and a maximum gap size of 3. Afterwards, X, Y, and Z coordinates of

each spot at all time points were used to quantify telomere movements. Inter-telomere distances were calculated for all telomeres of a representative nucleus based on differences in distance between time point 1 and time point 30. For this purpose, an inter-telomere distance matrix was generated for time point 1 (matrix1) and time point 30 (matrix30). We then calculated the change in inter-telomere distance by subtracting matrix1 from matrix30. The resulting matrix was then visualized as a heatmap generated in RStudio using the heatmap2 function of the gplots package. Distances are presented in µm and visualized by two different colours indicating an increase (green) or decrease (red) of inter-telomere distance over time.

3D stacks of 12 live nuclei were semi-automatically segmented and triangulated surfaces of nuclear boundaries were generated using Amira 4.1 (Mercury Computer Systems, San Diego, USA). To account for relative nuclear movements (i.e., translations, rotations), 3D point clouds of telomere mass centers from subsequent time points (t>0) were rigidly registered to the reference system of coordinates given by the first time point (t=0) using absolute orientation quaternions (Horn 1987). To characterize the intranuclear telomere motion, the MSD of telomeres relatively to their initial position (t=0) was calculated as

$$MSD(t) = \frac{1}{N} \sum_{i=1}^{N} (R_i(t) - R_i(0))^2$$
, Eq. 1

where $R_i(t)$ denote the radius vector of the *i-th* registered telomere in the reference system of coordinates at the time point t>0. Intranuclear position of telomeres was quantified in three representative nuclei by the shortest distance (D, um) between the telomere mass center and the nuclear envelope as well as the normalized radial distance (NRD)

$$NRD = TN/BN$$
.

where TN and BN are the Euclidean distances between nuclear envelope (N), telomere (T) mass centers and the intersection point of the $N \rightarrow T$ line with the nuclear envelope surface (B), respectively. Accordingly, small NRD values indicate nuclear-central telomere location, while values close to 1 correspond to the nuclear periphery.

Acknowledgements

We would like to acknowledge Uwe Sonnewald (Friedrich-Alexander University Erlangen-Nuremberg, Germany) for providing us with pUL50-GFP. We are also thankful to Martina Dvořáčková and Jiří Fajkus (Institute of Biophysics, Brno, Czech Republic) for providing us with TRB1-GFP. This work was supported by the DFG (Grant DFG HO1779/22-1, HO1779/28-1) to A.H.) and the European Research Council (Advanced Grant COMREC 26852 to H.P.) No conflict of interest exists.

Short legends for Supporting Information

Supplementary File 1 Telomere FISH on N. benthamiana chromosomes

Supplementary File 2 Telomere FISH on *N. benthamiana* wild-type interphase nucleus.

Supplementary File 3 Dynamic Imaging of telomeres by CRISPR-dCas9

Supplementary File 4 3D telomere localization

Supplementary File 5 Telomere tracking

This article is protected by copyright. All rights reserved.

Supplementary File 6 Registration of telomere movements to reference system

Supplementary File 7 Primers used for T-DNA construction

References

- Anton, T., Bultmann, S., Leonhardt, H. and Markaki, Y. (2014) Visualization of specific DNA sequences in living mouse embryonic stem cells with a programmable fluorescent CRISPR/Cas system. *Nucleus*, **5**, 163-172.
- Belhaj, K., Chaparro-Garcia, A., Kamoun, S. and Nekrasov, V. (2013) Plant genome editing made easy: targeted mutagenesis in model and crop plants using the CRISPR/Cas system. *Plant methods*, **9**.
- Boch, J., Scholze, H., Schornack, S., Landgraf, A., Hahn, S., Kay, S., Lahaye, T., Nickstadt, A. and Bonas, U. (2009) Breaking the code of DNA binding specificity of TAL-type III effectors. *Science*, **326**, 1509-1512.
- Boettiger, A.N., Bintu, B., Moffitt, J.R., Wang, S., Beliveau, B.J., Fudenberg, G., Imakaev, M., Mirny, L.A., Wu, C.T. and Zhuang, X. (2016) Super-resolution imaging reveals distinct chromatin folding for different epigenetic states. *Nature*, 529, 418-422.
- **Bonev, B. and Cavalli, G.** (2016) Organization and function of the 3D genome. *Nat Rev Genet*, **17**, 661-678.
- Chen, B., Gilbert, L.A., Cimini, B.A., Schnitzbauer, J., Zhang, W., Li, G.W., Park, J., Blackburn, E.H., Weissman, J.S., Qi, L.S. and Huang, B. (2013) Dynamic imaging of genomic loci in living human cells by an optimized CRISPR/Cas system. *Cell*, **155**, 1479-1491.
- Chen, B., Guan, J. and Huang, B. (2016a) Imaging Specific Genomic DNA in Living Cells. *Annual review of biophysics*, **45**, 1-23.
- Chen, B., Hu, J., Almeida, R., Liu, H., Balakrishnan, S., Covill-Cooke, C., Lim, W.A. and Huang, B. (2016b) Expanding the CRISPR imaging toolset with Staphylococcus aureus Cas9 for simultaneous imaging of multiple genomic loci. *Nucleic acids research*, **44**, e75.
- Chen, B.H., Hu, J., Almeida, R., Liu, H., Balakrishnan, S., Covill-Cooke, C., Lim, W.A. and Huang, B. (2016c) Expanding the CRISPR imaging toolset with Staphylococcus aureus Cas9 for simultaneous imaging of multiple genomic loci. *Nucleic acids research*, 44.
- Cryderman, D.E., Morris, E.J., Biessmann, H., Elgin, S.C.R. and Wallrath, L.L. (1999) Silencing at Drosophila telomeres: nuclear organization and chromatin structure play critical roles. *Embo Journal*, **18**, 3724-3735.
- **Dolezel, J., Greilhuber, J. and Suda, J.** (2007) Estimation of nuclear DNA content in plants using flow cytometry. *Nat Protoc*, **2**, 2233-2244.
- Dvorackova, M., Rossignol, P., Shaw, P.J., Koroleva, O.A., Doonan, J.H. and Fajkus, J. (2010) AtTRB1, a telomeric DNA-binding protein from Arabidopsis, is

- concentrated in the nucleolus and shows highly dynamic association with chromatin. *Plant J*, **61**, 637-649.
- **Fajkus, J., Kovarik, A., Kralovics, R. and Bezdek, M.** (1995) Organization of Telomeric and Subtelomeric Chromatin in the Higher-Plant Nicotiana-Tabacum. *Molecular & General Genetics*, **247**, 633-638.
- **Fauser, F., Schiml, S. and Puchta, H.** (2014) Both CRISPR/Cas-based nucleases and nickases can be used efficiently for genome engineering in Arabidopsis thaliana. *Plant J*, **79**, 348-359.
- Fujimoto, S., Sugano, S.S., Kuwata, K., Osakabe, K. and Matsunaga, S. (2016) Visualization of specific repetitive genomic sequences with fluorescent TALEs in Arabidopsis thaliana. *J Exp Bot*, **67**, 6101-6110.
- Gottschling, D.E., Aparicio, O.M., Billington, B.L. and Zakian, V.A. (1990) Position Effect at Saccharomyces-Cerevisiae Telomeres Reversible Repression of Pol-li Transcription. *Cell*, **63**, 751-762.
- **Horn, B.K.P.** (1987) Closed-Form Solution of Absolute Orientation Using Unit Quaternions. *J Opt Soc Am A*, **4**, 629-642.
- Ishii, T., Sunamura, N., Matsumoto, A., Eltayeb, A.E. and Tsujimoto, H. (2015)
 Preferential recruitment of the maternal centromere-specific histone H3 (CENH3)
 in oat (Avena sativa L.) x pearl millet (Pennisetum glaucum L.) hybrid embryos.

 Chromosome Res, 23, 709-718.
- Jinek, M., Chylinski, K., Fonfara, I., Hauer, M., Doudna, J.A. and Charpentier, E. (2012) A Programmable Dual-RNA-Guided DNA Endonuclease in Adaptive Bacterial Immunity. *Science*, **337**, 816-821.
- **Kato, N. and Lam, E.** (2001) Detection of chromosomes tagged with green fluorescent protein in live Arabidopsis thaliana plants. *Genome Biol*, **2**, RESEARCH0045.
- **Koo, D.H., Zhao, H.N. and Jiang, J.M.** (2016) Chromatin-associated transcripts of tandemly repetitive DNA sequences revealed by RNA-FISH. *Chromosome Research*, **24**, 467-480.
- Kozubek, S., Lukasova, E., Amrichova, J., Kozubek, M., Liskova, A. and Slotova, J. (2000) Influence of cell fixation on chromatin topography. *Analytical biochemistry*, **282**, 29-38.
- Lamm, C.E., Link, K., Wagner, S., Milbradt, J., Marschall, M. and Sonnewald, U. (2016) Human Cytomegalovirus Nuclear Egress Proteins Ectopically Expressed in the Heterologous Environment of Plant Cells are Strictly Targeted to the Nuclear Envelope. *Viruses-Basel*, 8.
- Lindhout, B.I., Fransz, P., Tessadori, F., Meckel, T., Hooykaas, P.J. and van der Zaal, B.J. (2007) Live cell imaging of repetitive DNA sequences via GFP-tagged polydactyl zinc finger proteins. *Nucleic Acids Res*, **35**, e107.
- Ma, H., Naseri, A., Reyes-Gutierrez, P., Wolfe, S.A., Zhang, S. and Pederson, T. (2015) Multicolor CRISPR labeling of chromosomal loci in human cells. *Proc Natl Acad Sci U S A*, **112**, 3002-3007.
- **Ma, H., Reyes-Gutierrez, P. and Pederson, T.** (2013) Visualization of repetitive DNA sequences in human chromosomes with transcription activator-like effectors. *Proc Natl Acad Sci U S A*, **110**, 21048-21053.

- Ma, H., Tu, L.C., Naseri, A., Huisman, M., Zhang, S., Grunwald, D. and Pederson, T. (2016) CRISPR-Cas9 nuclear dynamics and target recognition in living cells. J Cell Biol, 214, 529-537.
- Nimmo, E.R., Cranston, G. and Allshire, R.C. (1994) Telomere-Associated Chromosome Breakage in Fission Yeast Results in Variegated Expression of Adjacent Genes. *Embo Journal*, **13**, 3801-3811.
- **Pacher, M. and Puchta, H.** (2016) From classical mutagenesis to nuclease-based breeding directing natural DNA repair for a natural end-product. *Plant J.*
- **Phan, H.T. and Conrad, U.** (2016) Plant-Based Vaccine Antigen Production. *Methods Mol Biol*, **1349**, 35-47.
- Piatek, A., Ali, Z., Baazim, H., Li, L., Abulfaraj, A., Al-Shareef, S., Aouida, M. and Mahfouz, M.M. (2015) RNA-guided transcriptional regulation in planta via synthetic dCas9-based transcription factors. *Plant Biotechnol J*, **13**, 578-589.
- **Puchta, H.** (2016a) Applying CRISPR/Cas for genome engineering in plants: the best is yet to come. *Curr Opin Plant Biol*, **36**, 1-8.
- **Puchta, H.** (2016b) Using CRISPR/Cas in three dimensions: towards synthetic plant genomes, transcriptomes and epigenomes. *Plant J*, **87**, 5-15.
- Qi, L.S., Larson, M.H., Gilbert, L.A., Doudna, J.A., Weissman, J.S., Arkin, A.P. and Lim, W.A. (2013) Repurposing CRISPR as an RNA-guided platform for sequence-specific control of gene expression. *Cell*, **152**, 1173-1183.
- Qin, P., Parlak, M., Kuscu, C., Bandaria, J., Mir, M., Szlachta, K., Singh, R., Darzacq, X., Yildiz, A. and Adli, M. (2017) Live cell imaging of low- and non-repetitive chromosome loci using CRISPR-Cas9. *Nat Commun*, **8**, 14725.
- Sanchez Moran, E., Armstrong, S.J., Santos, J.L., Franklin, F.C. and Jones, G.H. (2001) Chiasma formation in Arabidopsis thaliana accession Wassileskija and in two meiotic mutants. *Chromosome Res*, **9**, 121-128.
- Schrumpfova, P.P., Schorova, S. and Fajkus, J. (2016) Telomere- and Telomerase-Associated Proteins and Their Functions in the Plant Cell. *Frontiers in plant science*, **7**.
- Schrumpfova, P.P., Vychodilova, I., Dvorackova, M., Majerska, J., Dokladal, L., Schorova, S. and Fajkus, J. (2014) Telomere repeat binding proteins are functional components of Arabidopsis telomeres and interact with telomerase. *Plant J*, 77, 770-781.
- **Schubert, V., Rudnik, R. and Schubert, I.** (2014) Chromatin associations in Arabidopsis interphase nuclei. *Frontiers in genetics*, **5**, 389.
- Shao, S., Zhang, W., Hu, H., Xue, B., Qin, J., Sun, C., Sun, Y., Wei, W. and Sun, Y. (2016) Long-term dual-color tracking of genomic loci by modified sgRNAs of the CRISPR/Cas9 system. *Nucleic Acids Res*, **44**, e86.
- Steinert, J., Schiml, S., Fauser, F. and Puchta, H. (2015) Highly efficient heritable plant genome engineering using Cas9 orthologues from Streptococcus thermophilus and Staphylococcus aureus. *Plant J*, **84**, 1295-1305.
- Zetsche, B., Gootenberg, J.S., Abudayyeh, O.O., Slaymaker, I.M., Makarova, K.S., Essletzbichler, P., Volz, S.E., Joung, J., van der Oost, J., Regev, A., Koonin, E.V. and Zhang, F. (2015) Cpf1 is a single RNA-guided endonuclease of a class 2 CRISPR-Cas system. *Cell*, **163**, 759-771.

Zhou, Y., Wang, P., Tian, F., Gao, G., Huang, L., Wei, W. and Xie, X.S. (2017) Painting a specific chromosome with CRISPR/Cas9 for live-cell imaging. *Cell Res*, 27, 298-301.

Figure legends

Figure 1 Structure of the CRISPR-dCas9 construct

- (a) Transcription of Sp/Sa-dCas9 was initiated by the parsley ubiquitin 4 promoter and terminated by the pea 3A terminator. A SV40 NLS DNA sequence was used for nuclear localization of dCas9. Transcription of the sgRNA scaffold was initiated by the Arabidopsis ubiquitin 6 promoter.
- (b) Protospacer design for Sp-dCas9 and Sa-dCas9 to target telomere DNA sequence. Target sequence is shown in red. NGG protospacer adjacent motif (PAM) for Sp-dCas9 is indicated in blue whereas NGGGT PAM for Sa-dCas9 is indicated in green.

Figure 2 Live imaging of telomeres by CRISPR-dCas9

(a) Sp-dCas9-mRuby and sgRNA-telomere were used for live imaging of telomeres in *N. benthamiana* leaf cells during interphase (n=50). (b) As a negative control, sgRNA-telomere was omitted. (c-e) Immunofluorescence staining against Sp-dCas9-eGFP (c) combined with FISH against telomeres (d) and overlay to confirm co-localization (e). (f) Whisker-box-plot showing the efficiency of Sp-dCas9 to label telomeres (n=50). CRISPR live refers to the number of signals in live leaf nuclei whereas CRISPR fixed refers to the number of signals in isolated nuclei after fixation. -sgRNA indicates the number of telomeres counted after transformation of dCas9 without sgRNA-telomere.

This article is protected by copyright. All rights reserved.

(g) Intensity plot showing a positive correlation between FISH (red) and CRISPRimaging (green) regarding the size and intensity of hybridization signals (indicated by dotted line in (e)) (n=30). Scale bar equals 10 μm.

Figure 3 FRAP analysis demonstrates stable association of dCas9 with target sequence during interphase

FRAP experiments were conducted on three individual nuclei. A region of interest was bleached (indicated by arrows) and fluorescence intensity was compared to background fluorescence intensity to determine relative fluorescence intensity (RFI). Error bars represent standard deviation based on three biological replicates. Scale bar equals 10 µm.

Figure 4 CRISPR-dCas9 enables 3D tracking of telomeres and reveals long range movements during interphase

(a) Normalized radial distance (NDR) of telomeres of a representative nucleus. A NDR of 0 indicates localization in the centre of the nucleus whereas a NDR of 1 indicates localization at the nuclear envelope. Error bars represent standard deviation based on measurements conducted at different time points (1 to 30 min). Telomere number represents individual telomere signals in a live nucleus. (b) Mean-square-displacement (MSD) in μm² was measured in 12 live nuclei with a total of 181 telomere signals over a period of 30 minutes. Error bars represent standard deviation. (c) Heatmap showing changes in inter-telomere distance over a period of 30 minutes in a representative

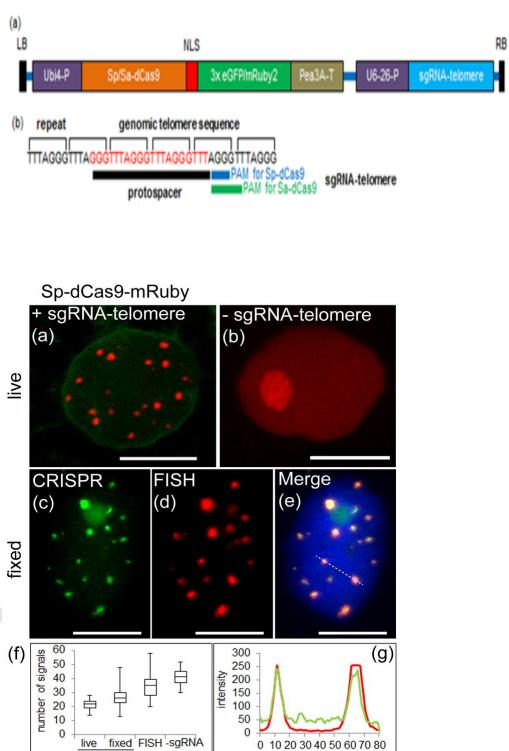
nucleus. Colours represent increased (green) and decreased (red) inter-telomere distance by up to 2 μ m. (d) 3D point clouds of telomeres of the same nucleus as in (c) from all time points rigidly registered to a reference system of coordinates given by time point 1.

Figure 5 Simultaneous visualization of telomeric DNA by CRISPR-dCas9 and the GFP-tagged telomeric repeat binding protein 1 (TRB1)

(a) Immunofluorescence staining against Sp-dCas9-mRuby2. (b) Immunofluorescence staining against TRB1-GFP. (c) Overlay showing almost complete co-localization except for putative blunt-ended telomeres (indicated by arrows). Scale bar equals 2 μm.

Figure 6 Comparison of Sa-dCas9 and Sp-dCas9

Telomeres were visualized by simultaneous application of two dCas9 orthologues (SadCas9 and Sp-dCas9). (a) Immunofluorescence staining against Sa-dCas9-eGFP. (b) Immunofluorescence staining against Sp-dCas9-mRuby2. (c) Overlay showing complete co-localization. (e) Quantification of the number of telomere signals observed by two different dCas9 orthologues (n=18). Scale bar equals 10 μm.



distance (pixels)

CRISPR

